

Structural and optical characterization of annealed $\text{As}_{30}\text{Te}_{60}\text{Ga}_{10}$ thin films prepared by thermal evaporation technique

A.M. ABD-ELNAIEM^{1,*}, M. MOHAMED¹, R.M. HASSAN^{1,2}, M.A. ABDEL-RAHIM¹,
A.A. ABU-SEHLY¹, M.M. HAFIZ¹

¹Physics Department, Faculty of Science, Assiut University, 71516 Assiut, Egypt

²Physics Department, Faculty of Education-Zingiber, Aden University, Yemen

Effect of annealing temperature on the structural and optical properties of $\text{As}_{30}\text{Te}_{60}\text{Ga}_{10}$ thin film was studied using various techniques such as differential scanning calorimetry (DSC), X-ray diffraction (XRD) and scanning electron microscopy (SEM). The DSC analysis revealed that the $\text{As}_{30}\text{Te}_{60}\text{Ga}_{10}$ glass has a single glass transition and crystallization peak while XRD results confirmed that the as-prepared and annealed films have crystalline nature. The coexistence of the crystalline phases in the investigated films could be attributed to the formation of orthorhombic As, hexagonal $\text{Ga}_7\text{Te}_{10}$, and monoclinic As_2Te_3 phases. It was found that the average crystallite size and optical parameters of the studied films depend on the annealing temperature. For example, the optical band gap decreased from 1.54 eV to 1.11 eV as the annealing temperature increased from 300 K to 433 K.

Keywords: *chalcogenide; As-Te-Ga; thin films; structural properties; optical properties; thermal evaporation*

1. Introduction

Chalcogenide glasses have received much attention due to their promising electronic properties. They are used for the electronic applications such as switching devices, infrared optical elements, optical fibers, optical transmission media, reversible phase change and optical records [1, 2]. The performance of these glasses, just like many other materials, largely depends on material preparation and heat treatment history. By extension, the performance of these materials can be enhanced if processing parameters are appropriately tuned. Arsenic-tellurium (As-Te) belongs to the archetypical chalcogenide glass-forming system characterized by high crystallization ability. As-Te glass shows a semiconductor-metal transition in the melt at relatively low temperatures [3]. Bulk As-Te glasses with a random covalent network, can be synthesized by melt quenching technique over a wide compositional range (20 at.% to

60 at.% As) [4]. In addition, As-Te thin films have been prepared by different methods, such as sputtering, thermal evaporation and wet chemistry techniques [5, 6]. Among them, the thermal evaporation technique is very common due to its simplicity, low-cost, reproducibility and scalability. Moreover, the thin films prepared by this method can adhere easily to the substrates.

The influence of thermal annealing on the optical properties of As-Te thin films has been interpreted based on the density of states model [7]. Early studies on the effect of thermal annealing on the structural and thermal properties [8–14] as well as glass-forming ability [15, 16] have been reported. While As-rich glasses show strong covalent bonds, the presence of threefold coordinated Te site enhances the metallic character and weakens the difference between the crystalline and glass states in Te-rich glasses.

Recently, few studies on the binary As-Te glasses and As-Te doped with another element(s) have been documented [17–23]. For example,

*E-mail: abd-elnaiem@aun.edu.eg

the optical gap of the as-prepared As-Te-Ag thin film was found to decrease with increasing Ag content, while the tail width of the localized states increased with Ag [11]. Alloying As-Te glass with Si makes it useful as a selector device in the memory array while doping with Ga enhances its electrical switching response [17]. The addition of Cu and Ge increases the glass transition temperature of the Cu-As-Te and Ge-As-Te glasses, respectively [18]. Moreover, the metallization pressure of Al-As-Te glasses increases with increasing Al content, which can be used to induce semiconductor-metal transformation [12]. To the best of our knowledge, optical and thermal properties of As-Te-Ga system have not been extensively studied [23]. This work reports an experimental study of the structural and optical properties of $As_{30}Te_{60}Ga_{10}$ thin films deposited by thermal evaporation.

2. Experimental

The bulk glass of $As_{30}Te_{60}Ga_{10}$ composition was prepared by the direct reaction of As, Te and Ga (99.999% purity) by melt quenching technique. The desired amounts of these elements were weighed and then sealed in the silica-glass ampoules under a vacuum of 1.33×10^{-3} Pa. The sealed ampoule was heated to 1100 K and held for 24 h. The melts were frequently stirred and thereafter quenched in cold water to get the glassy state of the studied composition. The stoichiometry of the $As_{30}Te_{60}Ga_{10}$ bulk glass was examined by energy dispersive X-ray spectroscopy, while the phase change was monitored with differential scanning calorimeter (DSC, Model: TA-Q20) under a nitrogen atmosphere. For this purpose, ~ 15 mg sample was observed under non-isothermal conditions with a heating rate of 10 K/min within the temperature range of 300 K to 675 K.

The $As_{30}Te_{60}Ga_{10}$ thin film was deposited by thermal evaporation method on cleaned soda-lime glass substrates under a vacuum of 1.33×10^{-3} Pa using Edwards E-306 coating system. The thickness (150 nm) of thin films was recorded using a quartz crystal monitor. The thermal annealing was performed at different temperatures (373 K, 393 K,

413 K and 433 K) for 1 h under vacuum. A Philips X-ray diffractometer of 1710-type with $CuK\alpha$ radiation of the wavelength of 1.5418 \AA was used to examine the structure of the as-prepared and annealed thin film of $As_{30}Te_{60}Ga_{10}$. The surface microstructure was observed by using JOEL-JSM-5400LV scanning electron microscope (SEM). The optical transmittance T and reflectance R of the $As_{30}Te_{60}Ga_{10}$ thin film measured at room temperature using a double-beam (SHIMADZU UV-2101) computer-controlled spectrophotometer in the wavelength between 200 nm and 2500 nm. The effect of the substrate on the optical parameters was excluded using a glass substrate as a reference during the optical measurements.

3. Theoretical background of structural and optical analyses

The crystal parameters, such as the average crystallite size (D_{hkl}) of the formed phases, can be estimated from the following equation [24, 25]:

$$D_{hkl} = \frac{K \lambda}{\beta_{hkl} \cos(\theta)} \quad (1)$$

where K is the Scherrer constant which equals unity for a minimum dislocation density, θ Bragg angle, λ wavelength of X-ray and β_{hkl} full width at half maximum intensity of the powder reflection peak.

The absorption coefficient α can be estimated from the experimentally measured values of $T(\lambda)$ and $R(\lambda)$ using the following relationship [26]:

$$\alpha = \frac{1}{d} \ln \left[\frac{(1-R)^2 + \sqrt{(1-R)^4 + 4(TR)^2}}{2T} \right] \quad (2)$$

where d is the film thickness. In the high absorption region, $\alpha \geq 10^4 \text{ cm}^{-1}$, the optical energy band gap E_g can be calculated using Tauc relation [7, 27]:

$$\alpha h\nu = B(h\nu - E_g)^r \quad (3)$$

where B is a constant which depends on the transition probability, and r is a number which determines the transition type ($r = 1/2$ and 2 for direct

and indirect allowed transition, respectively). In the exponential edge region, $10^4 \geq \alpha \geq 10^0 \text{ cm}^{-1}$, the absorption coefficient is governed by Urbach relation [28]:

$$\alpha(\nu) = \alpha_0 e^{\left(\frac{h\nu}{E_e}\right)} \quad (4)$$

where ν is the frequency of the radiation, α_0 is a constant and E_e is the Urbach energy interpreted as the width of the tails of localized states in the band gap.

To get a better understanding of the optical properties of the studied thin film other relevant parameters, such as the refractive index n , extinction coefficient k_{ex} , real ϵ_r and imaginary ϵ_i parts of dielectric constant, should be determined. The real part of dielectric constant is a measure of the speed of light inside the material, while the imaginary part is a measure of how dielectric absorbs energy from the electric field due to dipole motion. These parameters can be estimated by the following equations [29, 30]:

$$R = \frac{(n-1)^2 + k_{ex}^2}{(n+1)^2 + k_{ex}^2} \quad (5)$$

$$\epsilon_r = n^2 - k^2; \quad \epsilon_i = 2nk \quad (6)$$

$$k_{ex} = \frac{\alpha\lambda}{4\pi} \quad (7)$$

The dispersion energy is a measure of the strength of the interband optical transition and is related to the chemical bonding and the charge distribution within each unit cell. In addition, determination of the dispersion energy plays a major role in determining the behavior of the refractive indices and properly normalizes the interaction potential describing these optical effects which is due to the relationship between the electronic and optical properties of the material and its chemical bonds. The dispersion energy and oscillation energy are given by Wemple-Di Domenico relationship [31]:

$$(n^2 - 1)^{-1} = \frac{E_0}{E_d} - \frac{E^2}{E_d E_0} \quad (8)$$

where E_0 is the oscillation energy, E_d is the dispersion energy, and E is the photon energy of the incident light.

The high-frequency dielectric constant ϵ_∞ can be estimated via two procedures. The first one is to include the contribution of free carriers and lattice vibration modes of the dispersion as stated in equation 9 [32]:

$$n^2 = \epsilon_L - \left(\frac{e^2}{4\pi^2 c^2 \epsilon_0}\right) \left(\frac{N}{m^*}\right) \lambda^2 \quad (9)$$

where e is the charge of electron, ϵ_L is the dielectric constant, ϵ_0 is the permittivity of the free space ($8.854 \times 10^{-12} \text{ F/m}$), $\frac{N}{m^*}$ is the ratio between the free carrier concentration N and the effective electron mass m^* and c is the speed of light. The other approach is based on the dispersion arising from the bond carriers in the empty lattice. In this case, $\epsilon_L = n_\infty^2$ can be calculated using the single term Sellmeier oscillation [33]:

$$\frac{n_\infty^2 - 1}{n^2 - 1} = 1 - \left(\frac{\lambda_0}{\lambda}\right)^2 \quad (10)$$

where n_∞ is the long wavelength refractive index and λ_0 the average oscillator wavelength.

4. Results and discussion

4.1. Structural analysis

The DSC data shown in Fig. 1 reveal that the bulk As₃₀Te₆₀Ga₁₀ glass exhibits an endothermic glass transition, one distinct exothermic crystallization reaction, and endothermic melting peaks at 402.98 K, 495.22 K, 515.98 K, and 638.09 K, respectively. The observed glass transition temperature of the studied glass is higher than that of As₃₀Te₇₀ composition, which can be attributed to the increased connectivity due to the addition of Ga [6]. This observation agrees with other ternary systems, such as As-Te-In and As-Te-Al [12, 34]. However, the addition of Tl to As-Te-Tl system reduces glass transition temperature [35].

Fig. 2 shows the XRD spectra of the as-prepared and annealed samples. The as-prepared film exhibits the amorphous state with an appearance of a crystalline peak at $2\theta = 72.12^\circ$ which

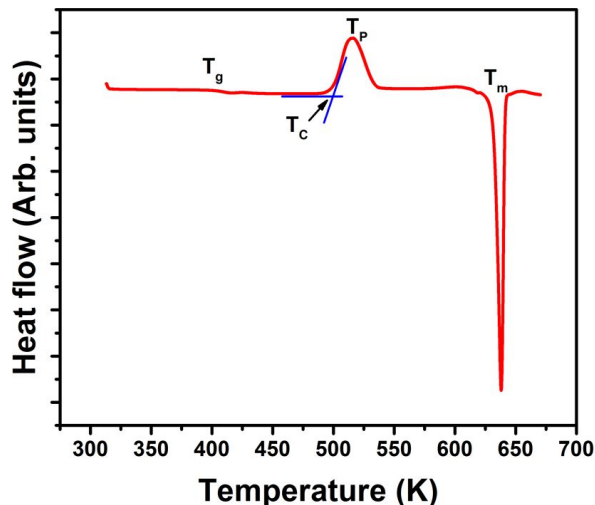


Fig. 1. DSC trace of $\text{As}_{30}\text{Te}_{60}\text{Ga}_{10}$ bulk glass at a heating rate of 10 K/min.

could be due to the crystallization of As during the film preparation. On the other hand, the XRD patterns of the crystallized films show the coexistence of As, $\text{Ga}_7\text{Te}_{10}$, and As_2Te_3 phases which have the orthorhombic, hexagonal and monoclinic crystal structures, respectively. The orthorhombic As phase has appeared in both the as-prepared and annealed films. However, the hexagonal phase of $\text{Ga}_7\text{Te}_{10}$ is observed in the samples annealed at 433 K and higher annealing temperatures, while the monoclinic phase of As_2Te_3 appears only in the films annealed at 473 K and other lower annealed temperatures. This means that the thermal annealing affects the structure of the studied films and results in amorphous-crystalline transformation in the annealed films. The estimated crystallite size values of the as-prepared and annealed $\text{As}_{30}\text{Te}_{60}\text{Ga}_{10}$ thin films, shown in Table 1, increase with the annealing temperature. This is an indication for increasing the crystallinity of the studied films with the thermal annealing.

The effect of thermal annealing on the morphology of the samples is shown in Fig. 3. For the as-prepared sample, As phase is found within the amorphous matrix (Fig. 3a). However, for the sample annealed at 433 K, which is located between the glass transition temperature and the crystallization peak region, many crystallites dispersed in the

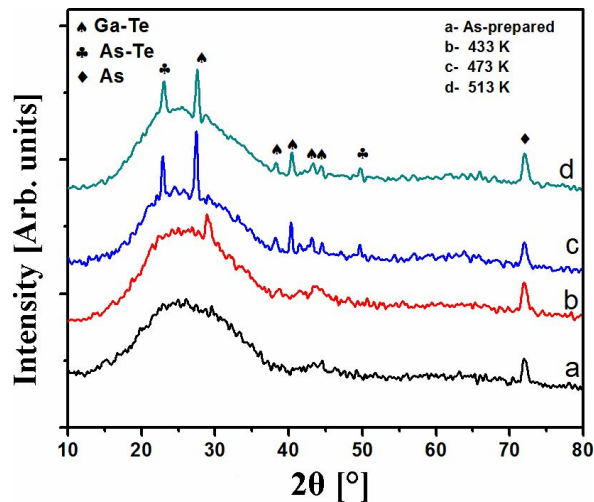


Fig. 2. X-ray diffraction patterns of the as-prepared and annealed $\text{As}_{30}\text{Te}_{60}\text{Ga}_{10}$ thin films.

amorphous matrix are observed (Fig. 3b). These crystallized particles could be related to the As and $\text{Ga}_7\text{Te}_{10}$ phases. Increasing the annealing temperature up to 473 K leads to a slight decrease in the particles size (Fig. 3c), which agrees with the XRD data of the studied films. Also, the particles number increases as the annealing temperature increases (Fig. 3c). This result could be attributed to the formation of the new As_2Te_3 phase in the annealed films. A further increase in the annealing temperature up to 513 K results in the formation of the crystallites with homogeneous distributions (Fig. 3d). For the samples annealed at 513 K, the crystallized particles of As, $\text{Ga}_7\text{Te}_{10}$, and As_2Te_3 phases are the result of high crystallization rate [16].

4.2. The optical analysis

The spectral distribution of the transmittance T and reflectance R of the as-prepared and annealed $\text{As}_{30}\text{Te}_{60}\text{Ga}_{10}$ thin films as a function of the wavelength of the incident light is shown in Fig. 4. In general, the transmittance decreases, while the reflectance increases with increasing the annealing temperature. Moreover, the reflectance increases with increasing the wavelength up to 835 nm and then decreases. The change in T and R indicates a change in the structure of the studied samples

Table 1. The observed, and standard ASTM values of the interplanar distances d , and calculated crystallite size (D_{hkl}) of the as-prepared and annealed $As_{30}Te_{60}Ga_{10}$ thin films.

Sample	Phase	(h k l)	Crystal structure	d [Å] observed	d [Å] ASTM	Crystallite	JCDS data file No.
						size, D_{hkl} [nm]	
As-prepared	As	(0 3 4)	O	1.312	1.310	12.4	85-1712
Annealed at 433 K	Ga_7Te_{10}	(2 4 1)	H	2.324	2.3242	24.77	85-0007
	As	(0 3 4)	O	1.312	1.310	10.73	85-1712
Annealed at 473 K	As_2Te_3	(1 1 0)	M	3.883	3.8745	19.89	87-0374
	Ga_7Te_{10}	(2 1 4)	H	3.248	3.2328	20.92	85-0007
	As_2Te_3	(5 1 3)	M	1.838	1.8388	25.61	87-0374
	As	(0 3 4)	O	1.312	1.310	13.57	85-1712
Annealed at 513 K	As_2Te_3	(1 1 0)	M	3.864	3.8699	15.69	75-1470
	Ga_7Te_{10}	(2 1 4)	H	3.238	3.2324	17.19	85-0007
	As_2Te_3	(5 1 3)	M	1.836	1.8365	22.70	72-1685
	As	(0 3 4)	O	1.311	1.310	12.98	85-1712

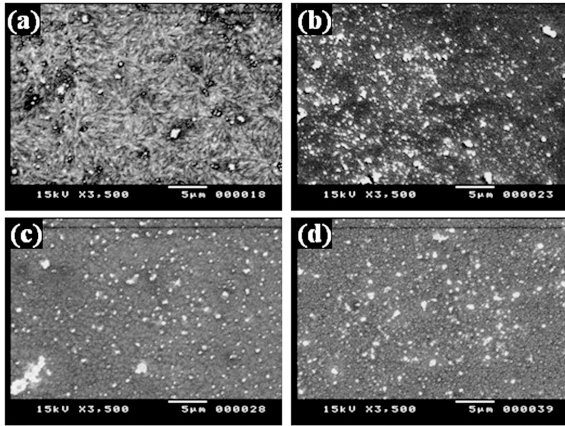


Fig. 3. SEM images showing the surface morphology of (a) as-prepared and annealed $As_{30}Te_{60}Ga_{10}$ films at: (b) 433 K, (c) 473 K, and (d) 513 K for 1 h.

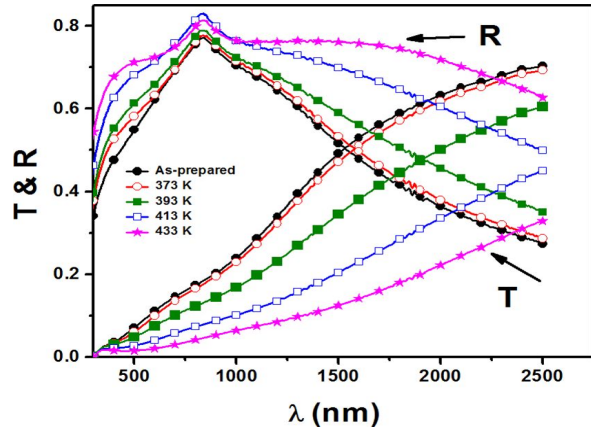


Fig. 4. The measured transmittance T and reflectance R of the as-prepared and annealed $As_{30}Te_{60}Ga_{10}$ thin films.

during the thermal annealing. The change in structure may lead to a change in the electronic properties.

Fig. 5 shows the dependence of the absorption coefficient α on the incident photon energy for the as-prepared and annealed films. The value of α , estimated using equation 2, was found to increase with increasing the annealing temperature. Fig. 6 shows the linear relationship between $(\alpha h\nu)^{1/2}$

and the photon energy $h\nu$ of the as-prepared and annealed thin films at the absorption edge. This result confirms the indirect band gap transition in $As_{30}Te_{60}Ga_{10}$ system and is in a good agreement with published work of other chalcogenide materials [37]. The optical energy gap of the indirect transition is obtained by extrapolating the linear portion of the curves shown in Fig. 6 to zero absorption. The values of the energy gap

decrease from 1.54 eV to 1.11 eV as the annealing temperature increases from 300 K to 433 K. This result could be explained in terms of the crystalline particles formed in the annealed films. At higher annealing temperature, the crystallite size decreases and strain value increases, leading to a decrease in the optical energy gap E_g [38]. In other words, increasing the number as well as size of the crystallite may result in localized states in the band structure, thereby decreasing the energy gap of the investigated system.

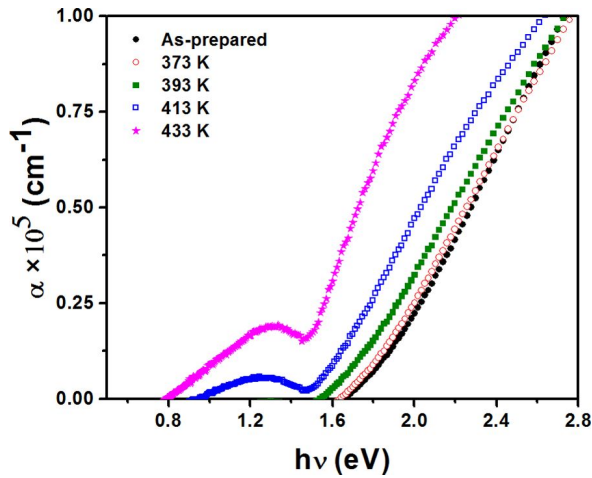


Fig. 5. The absorbance coefficient α of the as-prepared and annealed $\text{As}_{30}\text{Te}_{60}\text{Ga}_{10}$ thin films.

$\ln(\alpha)$ of the studied films against the photon energy is shown in Fig. 7. The values of the band width of localized states, E_c , obtained from the slope of the straight lines in Fig. 7, increase from 24 to 49 meV as the annealing temperature increase up to 433 K (see Fig. 8). The decrease in the optical energy gap E_g and the increase of localized states tails E_c with the annealing temperature can be interpreted based on the production of surface dangling bonds around the crystallites during the process of crystallization [39]. It has been suggested by many authors, that nearly ideal amorphous solids crystallize under the thermal annealing and accordingly the dangling bonds are produced around the surface of the crystallites [40]. Increasing the thermal annealing temperature of the thin films could cause a breaking of the crystallites into smaller crystals. This indicates increase in the number of

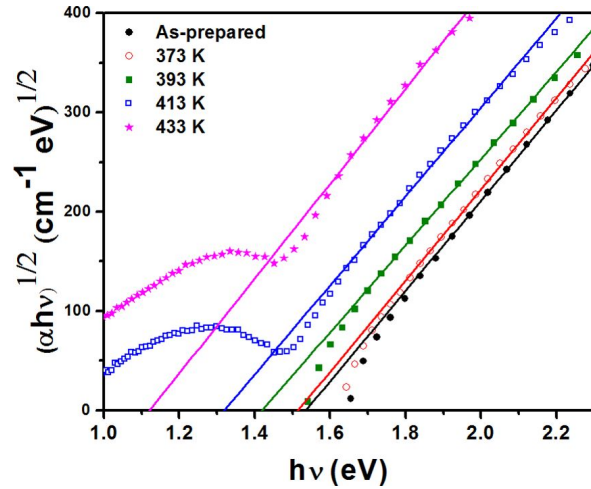


Fig. 6. Plot of $(\alpha h\nu)^{1/2}$ versus photon energy ($h\nu$) of the as-prepared and annealed $\text{As}_{30}\text{Te}_{60}\text{Ga}_{10}$ thin films. The straight lines are a linear fit of the absorption edges.

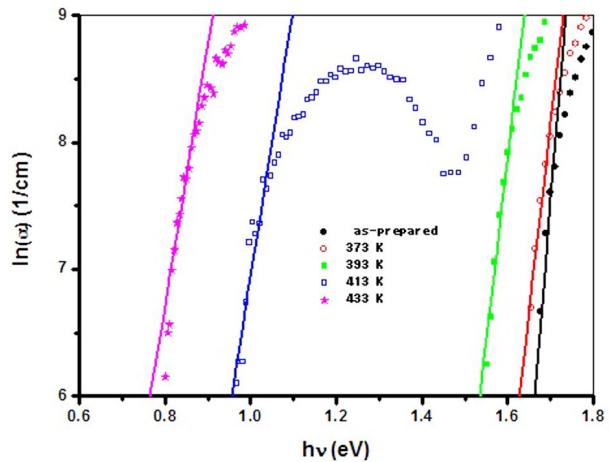


Fig. 7. Plot of $\ln\alpha$ versus photon energy $h\nu$ of the as-prepared and annealed $\text{As}_{30}\text{Te}_{60}\text{Ga}_{10}$ thin films. The straight lines are a linear fit of Urbach tails.

surface dangling bonds [40] which are responsible for the formation of some types of defects in the highly polycrystalline solids. Thus, the concentration of localized states in the band structure increases gradually as a result of increasing the dangling bonds in the annealed films. This could lead to an increase in the width of localized states, indicating a decrease in the optical energy gap of the investigated films.

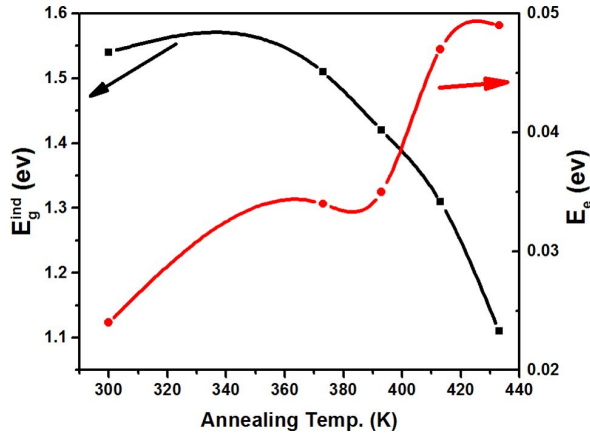


Fig. 8. Variation of the optical energy gap E_g and the bandwidth E_e versus the annealing temperature of the $As_{30}Te_{60}Ga_{10}$ thin films. The solid lines are guides to the eye.

The spectral dependence of the refractive index and extinction coefficient of the as-prepared and annealed $As_{30}Te_{60}Ga_{10}$ films on the wavelength of the incident light are shown in Fig. 9 and Fig. 10, respectively. The studied composition exhibits a high refractive index value of up to 20. The decrease in the refractive index with increasing the wavelength may be attributed to the effect of free carrier concentration. The thermal annealing results in an increase in the refractive index especially above $\lambda = 1000$ nm because the frozen network structure relaxes and further polymerizes. Also, the increase of the refractive index value can be attributed to the increased film density which agrees with the XRD data of the studied films. The values of n have a maximum value n_{max} at the wavelength λ_c (≈ 835 nm). The value of λ_c is independent of the annealing temperature as shown in Fig. 9. The increase in k_{ex} (Fig. 10) may be attributed to the increase in the average crystallites size with increasing annealing temperature of the studied films.

Furthermore, the variation of both real ϵ_r and imaginary ϵ_i parts of the dielectric constant of the as-prepared and annealed films with the wavelength is shown in Fig. 11 and Fig. 12, respectively. Both ϵ_r and ϵ_i show linear behavior at higher wavelengths. It is clearly seen that the values of n , k_{ex} ,

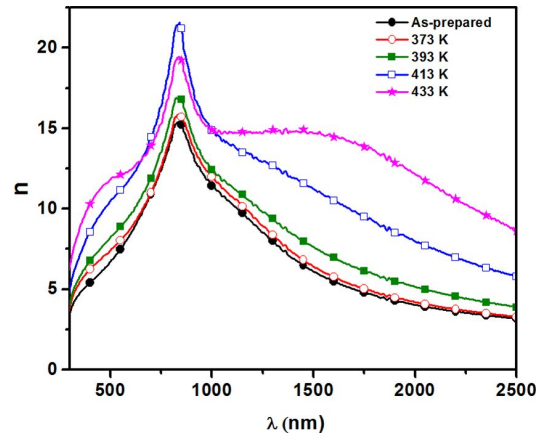


Fig. 9. The refractive index n versus wavelength λ of the as-prepared and annealed $As_{30}Te_{60}Ga_{10}$ thin films.

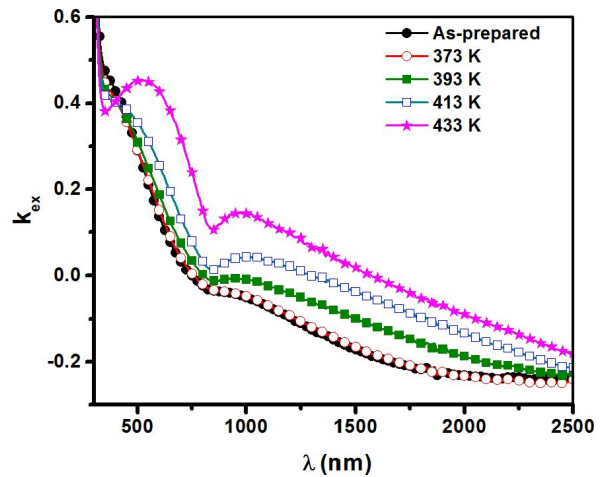


Fig. 10. The dependence of extinction coefficient k_{ex} on the wavelength λ for the as-prepared and annealed $As_{30}Te_{60}Ga_{10}$ thin films.

ϵ_r , and ϵ_i increase with annealing temperature. ϵ_r sharply decreases with increasing the wavelength above $\lambda = 840$ nm, while ϵ_i decrease with increasing the wavelength for all measured samples.

We evaluated the dispersion parameters of the investigated films to get more understanding of their optical properties. Plotting $(n^2 - 1)^{-1}$ against E^2 (Fig. 13) gives straight lines with a slope = $(E_0 E_d)^{-1}$ and intercept = E_0 / E_d . The estimated values of E_d and E_0 of our samples are listed in Table 2. It is observed that the values of E_0 decrease, while E_d increases with increasing the annealing

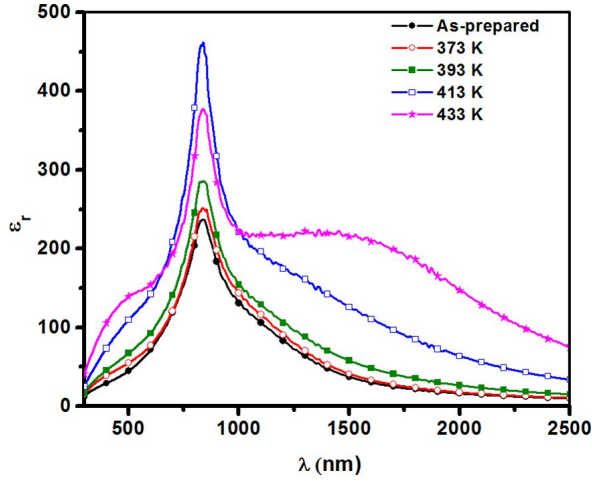


Fig. 11. Plots of the real part of the dielectric constant ϵ_r of the as-prepared and annealed $As_{30}Te_{60}Ga_{10}$ films versus wavelength λ .

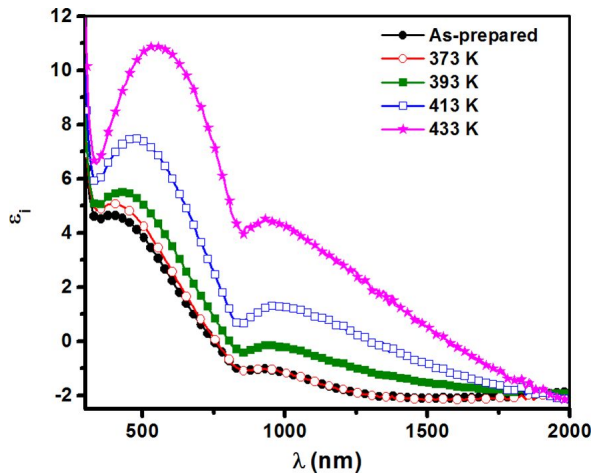


Fig. 12. Plots of the imaginary part of the dielectric constant ϵ_i versus wavelength of the as-prepared and annealed $As_{30}Te_{60}Ga_{10}$ thin films.

temperature. The decrease of E_0 and increase of E_d with the annealing temperature could be attributed to increasing the rate of atomic diffusion in the annealed thin films, indicating an increase in the number of atoms at interstitial sites which causes a formation of the impurity type scattering centers.

The plots of n^2 versus λ^2 of the studied films are shown in Fig. 14. By extrapolating the linear part of the curves to zero wavelength, the values of ϵ_L and $\frac{N}{m^*}$ were obtained and are given in Table 2. It can

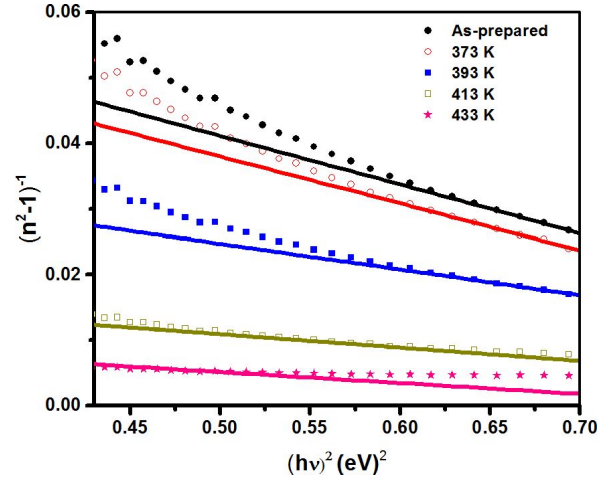


Fig. 13. Plot of $(n^2 - 1)^{-1}$ versus $(h\nu)^2$ of the as-prepared and annealed $As_{30}Te_{60}Ga_{10}$ thin films.

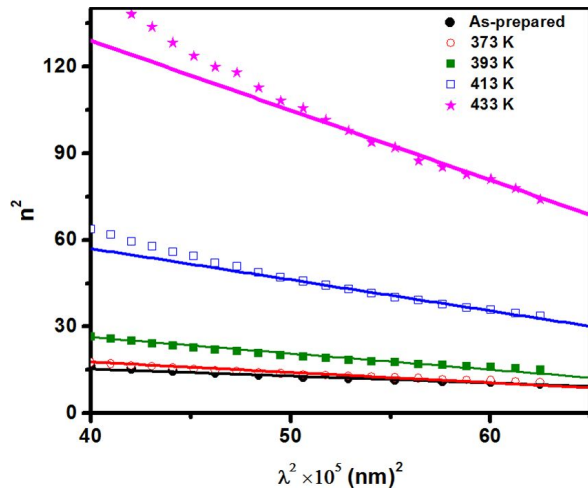
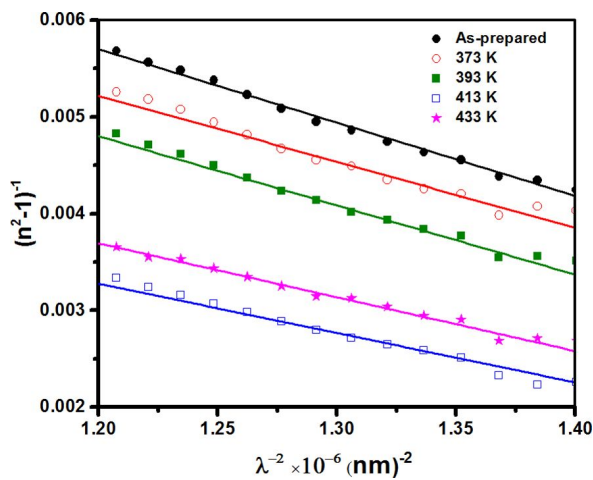
be seen that both ϵ_L and $\frac{N}{m^*}$ increase with the annealing temperature as observed in the literature for other chalcogenide glasses [27, 32, 37]. The dependence of ϵ_L and $\frac{N}{m^*}$ on the annealing temperature may be attributed to the increase in the free carrier concentration at higher annealing temperature. In general, it can be concluded that both the high frequency dielectric constant and the ratio $\frac{N}{m^*}$ are related to the internal microstructure of the studied composition. The value of the high-frequency dielectric constant ϵ_∞ can also be estimated from the plot of $(n^2 - 1)^{-1}$ against λ^{-2} (Fig. 15). These values are provided in Table 2. It is clear that the values of ϵ_L are higher than those of ϵ_∞ because of the increased carrier concentration.

5. Conclusions

$As_{30}Te_{60}Ga_{10}$ thin films were prepared by thermal evaporation and characterized with different techniques. The DSC results confirmed the glassy state of studied compositions. Analysis of XRD data revealed that the as-prepared thin films are amorphous in nature with possible As precipitations, while annealed thin films are polycrystalline. The observed phases are orthorhombic As, hexagonal Ga_7Te_{10} , and monoclinic As_2Te_3 . The optical analysis showed that the $As_{30}Te_{60}Ga_{10}$ thin film obeys the indirect electronic transition. It was

Table 2. The dispersion parameters of the as-prepared and annealed $As_{30}Te_{60}Ga_{10}$ thin films.

Annealing temperature [K]	E_o [eV]	E_d [eV]	λ_0 [nm]	$S_o \times 10^{13}$ [m^{-2}]	ϵ_L	ϵ_∞	$N/m^* \times 10^{57}$ [$m^{-3} \cdot kg^{-1}$]
As-prepared	1.22	13.13	715.95	13.13	24.88	11.76	2.97
373	1.21	13.76	723.69	14.62	32.07	12.37	4.42
393	1.16	24.04	731.21	14.96	48.68	21.72	6.89
413	1.11	66.28	736.87	19.58	100.03	60.71	13.26
433	1.02	48.25	732.68	17.94	108.58	47.31	15.13

Fig. 14. Plots of n^2 versus λ^2 of the as-prepared and annealed $As_{30}Te_{60}Ga_{10}$ thin films.Fig. 15. Plots of $(n^2 - 1)^{-1}$ versus λ^{-2} of the as-prepared and annealed $As_{30}Te_{60}Ga_{10}$ thin films.

found that the values of the band gap of the investigated films decrease as the annealing temperature increases. However, the reflectance, absorption coefficient, extinction coefficient, refractive index, real and imaginary part of the dielectric constant increase with increasing annealing temperature. In conclusion, the thermal annealing temperature is an important factor which can control the optical parameters of $As_{30}Te_{60}Ga_{10}$ and help in developing these materials for the potential use in technological applications.

References

- [1] ZALLEN R., PENCHINA C.M., *Am. J. Phys.*, 54 (1986), 862.
- [2] BURINA A., LECANTE P., MOSSET A., GALY J., TONNERRE J.M., RAOUX D., *J. Non-Cryst. Solids*, 212 (1997), 23.
- [3] ENDO H., HOSHINO H., IKEMOTO H., MIYANAGA T., *J. Phys.-Condens. Mat.*, 12 (2000), 6077.
- [4] KASEMAN D.C., HUNG I., LEE K., KOVNIR K., GAN Z., AITKEN B., SEN S., *J. Phys. Chem. B*, 119 (2015), 2081.
- [5] SEDDON A.B., *J. Non-Cryst. Solids*, 184 (1995), 44.
- [6] ABD-ELNAIEM A.M., MOHAMED M., HASSAN R.M., ABDEL-RAHIM M.A., ABU-SEHLY A.A., HAFIZ M.M., *Mater. Sci.-Poland*, 35 (2017), 335.
- [7] DAVIS E.A., MOTT N.F., *Philos. Mag.*, 22 (1970), 0903.
- [8] TVERJANOVICH A., YAGODKINA M., STRYKANOV V., *J. Non-Cryst. Solids*, 223 (1998), 86.
- [9] FAIGEL GY., GRANASY L., VINCZE I., WAARD DE H., *J. Non-Cryst. Solids*, 57 (1983), 411.
- [10] TOSCANI S., DUGUE J., CEOLIN R., *Thermochim. Acta*, 196 (1992), 191.
- [11] HAFIZ M.M., MOHARRAM A.H., ABU-SEHLY A.A., *Appl. Surf. Sci.*, 115 (1997), 203.
- [12] MURUGAVEL S., ACHARYA K.V., ASOKAN S., *J. Non-Cryst. Solids*, 191 (1995), 327.

- [13] QUINN R.K., *Mater. Res. Bull.*, 9 (1974), 803.
- [14] TITUS S.S.K., ASOKAN S., GOPAL E.S.R., *Solid State Commun.*, 83 (1992), 745.
- [15] CORNET J., ROSSIER D., *J. Non-Cryst. Solids*, 12 (1973), 85.
- [16] CORNET J., ROSSIER D., *J. Non-Cryst. Solids*, 12 (1973), 61.
- [17] KIM S., KIM H., CHOI S., *J. Alloy. Compd.*, 667 (2016), 91.
- [18] JOVARI P., LUCAS P., YANG Z., BUREAU B., KABAN I., BEUNEU B., PANATLEI C., BEDNARCIK J., *J. Non-Cryst. Solids*, 433 (2016), 1.
- [19] LUCAS P., COLEMAN G.J., KASEMAN D.C., YANG Z., HUNG I., GAN Z., SEN S., *J. Non-Cryst. Solids*, 432 (2016), 527.
- [20] TVERJANOVICH A., RODIONOV K., BYCHKOV E., *J. Solid State Chem.*, 190 (2012), 271.
- [21] DONGOL M., HAFIZ M.M., ABOU-ZIED M., ELHADY A.F., *Appl. Surf. Sci.*, 185 (2001), 1.
- [22] MANIKANDAN N., ASOKAN S., *J. Non-Cryst. Solids*, 353 (2007), 1247.
- [23] MOHAMED M., ABD-ELNAIEM A.M., HASSAN R.M., ABDEL-RAHIM M.A. HAFIZ M.M., *Appl. Phys. A*, 123 (2017), 511.
- [24] PATTERSON A.L., *Phys. Rev.*, 56 (1939), 978.
- [25] ABDEL-RAHIM M.N., ABDEL-LATIF A.Y., SOLTAN A.S., *Physica B*, 291 (2000), 41.
- [26] ABU EL-FADL A., HAFIZ M.M., WAKAAD M.M., AASHOUR A.S., *Radiat. Phys. Chem.*, 76 (2007), 61.
- [27] ABDEL-RAHIM M.A., *J. Phys. Chem. Solids*, 60 (1999), 29.
- [28] URBACH F., *Phys. Rev.*, 92 (1953), 1324.
- [29] VINCENT R.K., HUNT G.R., *Appl. Opt.*, 7 (1968), 53.
- [30] GRAVESTEIJN D.J., *Appl. Opt.*, 27 (1988), 736.
- [31] WEMPLE S.H., *Phys. Rev.B*, 7 (1973), 3767.
- [32] KHAN Z.H., ZULFEQUAR M., SHARMA T.P., HUSAIN M., *Opt. Mater.*, 6 (1996), 139.
- [33] LEE P.A., SAID G., DAVIS R., LIM T.H., *J. Phys. Chem. Solids*, 30 (1969), 2719.
- [34] KOSEK F., CIMPL Z., MIKHAILOV M.D., KARPOVA E.A., *J. Non-Cryst. Solids*, 86 (1986), 265.
- [35] SHARMILA B. H., ASOKAN S., *Appl. Phys. A*, 82 (2006), 345.
- [36] TU K.N., ROSENBERG R., *Analytical techniques for thin films: treatise on materials science and technology*, Elsevier, 2017.
- [37] MOHAMED M., MOUSTAFA S., ABD-ELNAIEM A.M., ABDEL-RAHIM M.A., *J. Alloy. Compd.*, 647 (2015), 771.
- [38] EL-SEBAILI A.A., KHAN S.A., AL-MARZOUKI F.M., FAIDAH A.S., AL-GHAMDI A.A., *J. Lumin.*, 132 (2012), 2082.
- [39] CHAUDHURI S., BISWAS S.K., CHOUDHURY A., GOSWAMI K., *J. Non-Cryst. Solids*, 54 (1983), 179.
- [40] HASEGAWA S., KITAGAWA M., *Solid State Commun.*, 27 (1978), 855.

Received 2016-12-22
Accepted 2018-02-13